JVI Journals.ASM.org

Identification and Characterization of a Proteolytically Primed Form of the Murine Coronavirus Spike Proteins after Fusion with the Target Cell

Oliver Wicht, Christine Burkard, Cornelis A. M. de Haan, Frank J. M. van Kuppeveld, Peter J. M. Rottier, Berend Jan Bosch

Virology Division, Department of Infectious Diseases and Immunology, Faculty of Veterinary Medicine, Utrecht University, Utrecht, The Netherlands

ABSTRACT

Enveloped viruses carry highly specialized glycoproteins that catalyze membrane fusion under strict spatial and temporal control. To prevent premature activation after biosynthesis, viral class I fusion proteins adopt a locked conformation and require proteolytic cleavage to render them fusion-ready. This priming step may occur during virus exit from the infected cell, in the extracellular milieu or during entry at or in the next target cell. Proteolytic processing of coronavirus spike (S) fusion proteins during virus entry has been suggested but not yet formally demonstrated, while the nature and functionality of the resulting subunit is still unclear. We used a prototype coronavirus—mouse hepatitis virus (MHV)—to develop a conditional biotinylation assay that enables the specific identification and biochemical characterization of viral S proteins on virions that mediated membrane fusion with the target cell. We demonstrate that MHV S proteins are indeed cleaved upon virus endocytosis, and we identify a novel processing product S2* with characteristics of a fusion-active subunit. The precise cleavage site and the enzymes involved remain to be elucidated.

IMPORTANCE

Virus entry determines the tropism and is a crucial step in the virus life cycle. We developed an approach to characterize structural components of virus particles after entering new target cells. A prototype coronavirus was used to illustrate how the virus fusion machinery can be controlled.

Enveloped viruses must fuse their envelope with a target cell membrane to get access to host cells and deliver their genetic information. They carry specialized surface glycoproteins that mediate attachment to and fusion with the host membrane. Viral fusion proteins can generally be divided into three distinct classes according to their molecular organization and fusion mechanism (1). Class I fusion proteins such as the influenza virus hemagglutinin and the human immunodeficiency virus Env occur as homotrimeric glycoproteins that are oriented perpendicular to the viral membrane and contain typical structural elements, including a receptor-binding domain, heptad repeat (HR) regions, an amphipathic fusion peptide (FP), and a C-terminal transmembrane domain (2). These fusion proteins also feature a common fusion mechanism (3). Initial conformational rearrangements triggered by cues such as receptor binding or low pH lead to the exposure and insertion of the FP into the target membrane. Subsequent structural reorganization pulls the two membranes together to achieve fusion. The free energy is provided by the S proteins and released by zipping up of the heptad repeat regions into an energetically favorable, stable six-helix bundle (1). To prevent premature activation, class I fusion proteins are produced in a locked conformation that needs proteolytic cleavage to acquire fusion competence. Cleavage typically occurs just upstream of the FP and causes N-terminal liberation thereof (4). Furin or furin-like proteases often prime the fusion proteins in the producer cell before virions are released. Alternatively, the cleavage event can take place after the release of virions from the infected cell, i.e., in the extracellular space or upon entry into new host cells (5–7). Prevention of fusion protein cleavage by mutagenesis of the cleavage site, as well as by inhibition of cellular proteases, often renders viruses noninfectious (8–10).

Coronavirus (CoV) entry is mediated by the spike (S) protein, an exceptionally large glycoprotein of approximately 1,200 to 1,450 amino acid residues in length that comprises the canonical structural features of class I fusion proteins and shares the typical fusion mechanism (11). The trimeric S proteins characteristically decorate the extracellular virus particles and two subunits of similar size can be distinguished. The N-terminal S1 subunit contains the receptor-binding domain, while the C-terminal S2 subunit comprises the fusion machinery, including a putative FP, HR regions, and transmembrane domain.

Some CoV S proteins are cleaved at the S1/S2 junction during biogenesis by furin(-like) proteases, but many CoVs lack a furin cleavage site at the S1/S2 junction and hence carry uncleaved S protein in their virions (12). Other cellular proteases have been reported to cleave CoV S proteins, but these proteases are only available upon attachment or during the uptake of virions by the next target cells (13). The infection of some CoVs can be blocked by protease inhibitors, thereby underlining the importance of proteolytic activation that should render class I fusion proteins into their fusion-competent form (6, 14–16). Remarkably, a cleavage at the S1/S2 junction does not liberate a putative FP at the N terminus of S2 (17). Rather than at the S1/S2 junction, cleavage

Received 22 November 2013 **Accepted** 20 February 2014

Published ahead of print 19 February 2014

Editor: S. Perlman

Address correspondence to Berend Jan Bosch, b.j.bosch@uu.nl.

Copyright © 2014, American Society for Microbiology. All Rights Reserved.

doi:10.1128/JVI.03451-13

Downloaded from http://jvi.asm.org/ on March 25, 2015 by Universiteitsbibliotheek Utrecht

can occur at alternative positions within the S2 domain of the protein to promote the fusion competence. Such alternative cleavage sites have been described within the S2 subunit for the S proteins of severe acute respiratory syndrome coronavirus (SARS)-CoV, mouse hepatitis virus (MHV), and infectious bronchitis virus (IBV) (16, 18, 19). In general, a variety of putative, alternative cleavage sites and cleavage timings have been reported or suggested for CoV, and yet the role of S protein cleavage remains largely undefined.

Despite extensive research on the proteolytic requirements for entry, the exact cleavage position within the CoV S protein generating the fusogenic subunit has been difficult to predict, and the formal demonstration of S protein cleavage upon entry is currently lacking. In the present study, we developed a novel unbiased approach to selectively identify and characterize the S proteins of incoming viruses that accomplish fusion. The assay employs a combination of a protein biotin ligase (BirA) and a biotin acceptor peptide added as an extension to the cytoplasmic tail of the S protein. When incoming viral proteins gain access to the cytoplasm of cells expressing BirA ligase, they are specifically labeled with biotin, which then enables isolation, enrichment, and detection. With this assay, we investigated the S glycoprotein of the prototype coronavirus MHV (strain A59). The MHV S proteins are partially cleaved into the noncovalently linked subunits at the S1/S2 junction by furin or furin-like proteases (20). Intriguingly, preventing furin cleavage by mutation or the use of furin inhibitors has no effect on virus infectivity of MHV (21–23). Using our new approach, we demonstrate that the MHV S proteins participating in fusion are proteolytically processed in the target cells at a different position in the S2 subunit. The newly identified S2* subunit has characteristics of the functional fusion machinery.

MATERIALS AND METHODS

Cells, viruses, antibodies, and HR2 peptide. HEK-293T, HeLa, Vero-CCL81, and LR7 (24) cells were maintained in Dulbecco modified Eagle medium supplemented with 10% fetal bovine serum. Generally, MHV (strain A59) was propagated and titrated in LR7 cells in culture medium supplemented with 20 mM HEPES. For the immune detection of S protein in virus supernatants, MHV was grown to high titers in Dulbecco modified Eagle medium supplemented with 0.3% tryptose phosphate broth (Sigma, catalog no. T9157). For immunoprecipitation (IP) and immune detection, MHV S protein was reacted with polyclonal rabbit anti-BAP antibody (GenScript, catalog no. A00674) or mouse monoclonal anti-S2 (10G) antibody and subsequently with anti-mouse or anti-rabbit immunoglobulin G conjugated to horseradish peroxidase (HRP; Dako, catalog no. P0217) (25, 26). A polyclonal rabbit anti-MHV serum (K135) was used to detect infected cells by reaction with anti-rabbit immunoglobulin G conjugated to HRP. Biotin was detected by streptavidin-HRP conjugate (Thermo Scientific, catalog no. 21126). The MHV fusion inhibitor HR2 peptide (DLSLDFEKLNVTLLDLTYEMNRIQDAIKKLNESYIN LKE) was synthesized by GenScript (11).

Construction of recombinant viruses. Recombinant MHVs were generated by targeted recombination as described earlier (27). A transfer vector based on pXHERLM was generated to create the recombinant MHV-BAP virus encoding a tandem repeat of the 15-amino-acid biotin acceptor peptide, including linkers DLPGGLNDIFEAQKIEWHEPPGGL NDIFEAQKIEWHE (the BAP sequence is underlined) as a C-terminal extension of the S protein (28). The recombinant viruses MHV^{FCS-}BAP and MHV^{S2*-}BAP were generated by introducing additional point mutations into the transfer vector using site-directed mutagenesis. MHV^{FCS-}BAP S protein carries three point mutations—R713S, R7174, and R717S—that substitute all arginines at the furin cleavage site by serines. MHV^{S2*}-BAP S protein carries two point mutations—R867S and R869S—that substitute the arginines at the putative S2′ cleavage site by serines.

Generation of stable cell lines. The pQCXIN-CCM plasmid encoding the MHV receptor, murine carcinoembryonic antigen-related cell adhesion molecule 1a (CCM), was generated by cloning the CCM gene into the pQCXIN Moloney murine leukemia virus (MLV) packaging vector (Clontech) (29). Likewise, the human codon-optimized gene encoding biotin protein ligase (BirA) with an N-terminal hemagglutinin and FLAG tag (the pUM376-BirA PCR template was kindly provided by V. Ogryzko) was cloned into the pQCXIP vector (Clontech), generating the pQCXIP-BirA packaging vector (30). HEK-293T, HeLa, and Vero-CCL81 cell lines expressing the CCM receptor were made after transduction with vesicular stomatitis virus G protein-pseudotyped MLV using the pQCXIN-CCM packaging vector. The polyclonal HEK-CCM, HeLa-CCM, and Vero-CCM cell lines stably expressing CCM, as well as murine LR7 cells, were selected and maintained with G418 (PAA). CCM expression was confirmed by immunodetection using mouse monoclonal anti-CCM antibody (MAb CC1, provided by K. Holmes [31]). Polyclonal LR7 cells stably expressing biotin protein ligase (LR7-BirA) were similarly made with the MLV-pseudotyped virus using the pQCXIP-BirA packaging vector. LR7-BirA cells were selected at 15 μg/ml and maintained at 10 μg of puromycin (Sigma, catalog no. P8833)/ml. BirA expression was confirmed by immunodetection using Cy3-conjugated mouse monoclonal anti-FLAG (Sigma, catalog no. A9594). No BirA enzyme was detected in the cell culture supernatants of LR7-BirA cells after 72 h of incubation, as analyzed by Western blotting with a mouse monoclonal anti-FLAG antibody conjugated to HRP.

Conditional biotinylation assay. LR7 or LR7-BirA cells were cultured to confluence in six-well clusters. Cells were inoculated with virus-containing cell culture supernatant supplemented with 50 μg of DEAE-dextran (Sigma, catalog no. D9885)/ml and 10 μM biotin (Sigma, catalog no. B4639) at a multiplicity of infection (MOI) of 10. After 30 min, protein biosynthesis was inhibited by the addition of 50 μg of cycloheximide (Sigma, catalog no. C7698)/ml to prevent S protein synthesis from virus infections. At 90 min postinfection (p.i.), the cells were chilled on ice, washed twice with ice-cold phosphate-buffered saline (PBS), and lysed in ice-cold radio immunoprecipitation assay (RIPA) buffer (150 mM NaCl, 1% Nonidet P-40, 0.5% sodium deoxycholate, 0.1% sodium dodecyl sulfate [SDS], 50 mM Tris-HCl [pH 8]) supplemented with Complete protease inhibitor cocktail tablets (Roche, catalog no. 11836153001) to prevent further proteolysis and with or without 6 mM sodium pyrophosphate (PP; Sigma, catalog no. 71516) to quench the activity of BirA in cell lysates (32). The cell lysates were cleared by centrifugation at 10,000 × *g* for 10 min at 4°C. The supernatants were combined with 20 μl of 50:50 slurry of protein G-Sepharose (Biovision, catalog no. 6511) supplemented with 0.5 mg of polyclonal anti-BAP antibody (GenScript, catalog no. A00674) and incubated under rotation for 2 h at 8°C to immunoprecipitate the S proteins. Next, Sepharose beads were pelleted at 6,000 × *g* for 5 min at 4°C and washed trice with an excess of ice-cold RIPA buffer. Excess supernatant was carefully removed, and samples were finally denatured by the addition of sample buffer and subjected to Western blotting.

If inhibitory compounds were used during the infection, cells were pretreated for 30 min at 37°C, followed by infection in the presence of the respective compounds. The following protease inhibitors were used at their highest recommended working range concentrations according to Sigma's protease inhibitor technical bulletin INHIB1 (final concentration): pepstatin A (1.5 μM; Sigma, P5318), leupeptin (100 μM, Sigma, catalog no. L2023), E64d (10 μM; Sigma, catalog no. E8640), phosphoramidon (10 μM; Sigma, catalog no. R7385), and AEBSF [4-(2-aminoethyl)-benzenesulfonyl fluoride; 100 μM; Sigma, catalog no. A8456]. HR2 peptide was used at 25 μM. The following lysosomotropic agents were used (final concentration): ammonium chloride (25 mM NH_4Cl; Merck, Darmstadt, Germany) and bafilomycin A1 (125 μM; Enzo Life Sciences).

Downloaded from http://jvi.asm.org/ on March 25, 2015 by Universiteitsbibliotheek Utrecht

Time course biotinylation assay. LR7 or LR7-BirA cells were cultured to confluence on 10-cm dishes, and the inoculum was prepared similar to the conditional biotinylation assay. First, cells were washed twice with ice-cold PBS, and ice-cold inoculum was added for 45 min to allow attachment of the virus to the target cells at 8°C. Next, the inoculum was removed, and the cell layer was washed once with ice-cold PBS, followed by the addition of 37°C culture medium supplemented with 10 μM biotin. Differential periods of infection were achieved by successively delaying the start of attachment and infection while maintaining an equal duration. All samples were harvested at the same time to even out the time between lysis and immunoprecipitation. Then, 50 μg of cycloheximide/ml was added 30 min after warming up the infection to 37°C for all samples with an infection period longer than 30 min or at the end of the infection. The sample for 0 min was prepared for lysis after 1 min at 37°C. Lysis and immunoprecipitation was performed as described in the conditional biotinylation assay, and IP samples were analyzed by Western blotting.

HR2 inhibition of MHV infection. Multiple wells containing LR7 cells were infected with wild-type MHV for 1.5 min to synchronize infection. The inoculum was replaced by culture medium at the start of infection. At increasing time points, supernatants of individual wells were replenished with culture medium supplemented with 20 μM HR2 peptide to block MHV entry. At 4 h p.i., the supernatant was replaced with culture medium containing 1 μM HR2 peptide to inhibit syncytium formation. At 7 h p.i., the cells were fixed with 3.7% formalin, immunoperoxidase staining was performed using K135 serum, and the cells were visualized using an AEC substrate kit (Vector Laboratories). The extent of infection relative to noninhibited virus infection was calculated from the number of plaques observed.

Deglycosylation. LR7 or LR7-BirA cells were cultured to confluence in 10-cm dishes, and the virus infection was performed similarly to that of the conditional biotinylation assay. After IP, samples on the Sepharose beads were denatured and deglycosylated with PNGase F (New England BioLabs, catalog no. P0704) according to the manufacturer's protocol. Finally, the samples were denatured by the addition of sample buffer and subsequently analyzed by Western blotting.

Western blot analysis. For the detection of S protein in virus-containing cell culture supernatants, aliquots were directly lysed and denatured in sample buffer containing 50 mM Tris-HCl (pH 6.8), 50% glycerol, 5% 2-mercaptoethanol, 1% SDS, and bromophenol blue and boiled at 95°C for 10 min. Samples after immunoprecipitation were eluted from beads by boiling at 95°C for 10 min in sample buffer. Supernatant was subjected to SDS-PAGE in a discontinuous gel with 8% acrylamide in the separating gel (33). Next, samples were transferred to a polyvinylidene fluoride membrane (Bio-Rad, catalog no. 162-0176). Membranes were blocked with bovine serum and reacted with antibodies or streptavidin-HRP in PBS with bovine serum and 0.5% Tween 20. For detection, we used an Amersham ECL Western blot analysis system (GE Healthcare, catalog no. RPN2109) with X-Omat LS films (Kodak; Sigma, catalog no. F1149).

Computational analysis. The transmembrane domain of MHV S protein was predicted by TMHMM 2.0, and the signal peptide was predicted by SignalP 4.1. HR1 and HR2 regions were defined according to the method of Bosch et al. (11). Glycosylation sites were predicted with NetNGlyc 1.0 (Technical University of Denmark). Western blot signals were quantified by using ImageJ. Amino acid sequence alignment was performed by CLUSTAL W2 using S sequences of infectious bronchitis virus (IBV strain Beaudette, NP_040831.1), Middle East respiratory syndrome coronavirus (MERS-CoV; strain HCoV-EMC, AFS88936.1), mouse hepatitis virus (MHV strain 2, AAF19386.1 and strain MHV-A59, NP_045300.1), severe acute respiratory syndrome coronavirus (SARS-CoV strain Tor2, NP_828851.1), and transmissible gastroenteritis virus (TGEV strain TO14, AF302263_1).

RESULTS

Biotinylation assay to label S protein after virus-cell fusion. During inoculation, not all virions successfully fuse with the target cell and deliver their genome into the cytoplasm. According to the current model of class I protein fusion, the C-terminal tail of the CoV S protein is hidden internally in the intact virion. It will be introduced into the cytoplasm after the virus and cell membrane have fused. In order to be able to discriminate S proteins coming from virions that successfully achieved fusion from those that failed, we designed a biotinylation assay that uses selective intracellular biotin labeling of the protein's C terminus. To that end, we generated a recombinant MHV-A59 derivative carrying an S protein with a C-terminally appended 37-amino-acid biotin acceptor peptide (MHV-BAP; Fig. 1A) and a recombinant murine cell line that constitutively expresses BirA in its cytoplasm (LR7-BirA). BirA recognizes the biotin acceptor peptide (BAP) as the substrate for biotin ligation in the presence of ATP and free biotin. In intact virions, the BAP faces the luminal side and is protected from modification by BirA, but upon virus-cell fusion it becomes exposed to the enzyme (Fig. 1B). Consequently, BirA can biotinylate the BAP tag of S proteins of virions that underwent fusion, enabling the selection and characterization of postfusion S proteins via the biotin label. MHV-BAP displayed similar growth kinetics but yielded 10-fold-reduced titers compared to wild-type MHV (data not shown).

To characterize the S protein of MHV-BAP and to demonstrate biotinylation of the BAP tag, we propagated wild-type MHV and the recombinant MHV-BAP in LR7 cells and LR7-BirA cells. The cell culture supernatants were analyzed by Western blotting with antibodies recognizing the S2 subunit or the BAP tag, or with the biotin-binding streptavidin (Fig. 1C). The monoclonal antibody recognizing the S2 subunit detected the full-length S protein (S_0) and the S2 subunit of all virus preparations. A polyclonal antibody directed against the BAP specifically detected S_0 and the S2 subunit of MHV-BAP but not those of wild-type MHV. Importantly, biotinylation of BAP-tagged S protein was only detected for MHV-BAP viruses produced in LR7-BirA cells, demonstrating the BirA-dependent biotinylation of the BAP. Recognition of the BAP by the anti-BAP polyclonal antibody was not influenced by its biotinylation status; tagged and nontagged S proteins were detected equally efficient.

Biotinylated S proteins after virus-cell fusion: detection of S2*. Next, we assessed the biotinylation of S proteins after membrane fusion of virions with BirA expressing target cells. The LR7-BirA cells were inoculated with MHV-BAP (MOI = 10) for 90 min to enable binding and fusion. To detect the biotinylated S proteins, anti-BAP antibody was used to immunoprecipitate the BAP-tagged S proteins from whole-cell lysates. This purification and concentration step was essential for detection. The BirA enzyme maintains its activity in the lysis buffer, even at low temperatures. Consequently, all S protein present in the cell lysate became biotinylated postlysis and could be detected using the streptavidin-HRP conjugate (Fig. 2A, lane 1). In addition to the S_0 and S2 forms, which could already be observed in the virus stock (Fig. 1C), an additional product of ~80 kDa was detected which we named S2*. To prevent postlysis biotinylation and analyze the S proteins as they occur in the intact cell, BirA activity was quenched by product feedback inhibition by the addition of PP to the lysis buffer and during the IP procedure (Fig. 2A, lane 2) (32). The S2* was the most abundant S protein product detected, and only limited amounts of S_0 and S2 were observed.

To test whether the appearance of the S2* protein indeed correlates with successful infection, we exploited the HR2 peptide, a

Downloaded from http://jvi.asm.org/ on March 25, 2015 by Universiteitsbibliotheek Utrecht

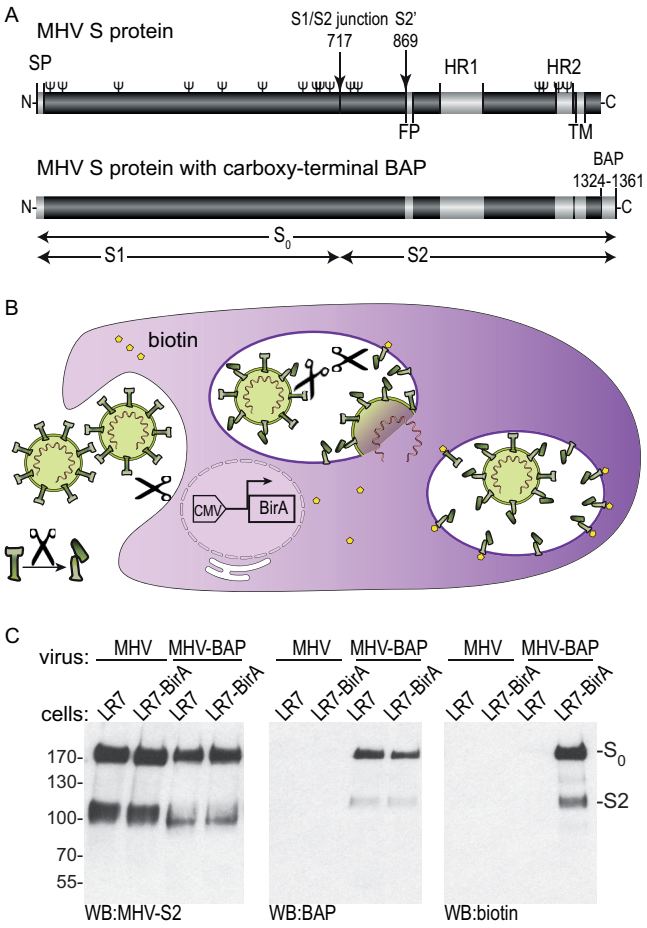

FIG 1 Recombinant MHV-BAP for the detection of biotinylated S proteins. (A) Schematic organization of wild-type (1,324 amino acids) and BAP-tagged MHV (strain A59) S protein (1,361 amino acids) drawn to scale. The S protein has an N-terminal S1 domain, responsible for receptor binding, and a C-terminal S2 domain that holds the fusion machinery. The positions of the signal peptide (SP), the predicted N-glycosylation sites (Ψ), the putative fusion peptide (FP), two heptad repeat (HR) regions, the transmembrane domain (TM), and the biotinylation acceptor peptide (BAP) are indicated. MHV S protein contains two predicted protease cleavage sites: a furin cleavage site at the S1/S2 junction and a putative second cleavage site (S2′) just upstream of the fusion peptide. (B) A biotinylation assay was designed to selectively identify and characterize the S protein of MHV virions that underwent membrane fusion with the cellular target membrane. The biotin acceptor peptide was fused to the C terminus of the S protein. Target cells stably express cytoplasmic protein biotin ligase (BirA) from a cytomegalovirus promoter. Upon membrane fusion, the C-terminal BAP of S protein is introduced into the cytoplasm and can be accessed and biotinylated by BirA. (C) Characterization of recombinant MHV-BAP. Virus stocks of MHV-A59 with wild-type S protein (MHV) or with BAP-tagged S protein (MHV-BAP) were produced in LR7 cells or LR7 cells expressing BirA (LR7-BirA) and subjected to Western blotting (WB) using a MHV-S2 monoclonal antibody, an anti-BAP polyclonal antibody, and streptavidin-HRP for the detection of proteins. Full-length S protein (S_0) and S2 subunit resulting from cleavage at the S1/S2 junction were detected with antibodies directed against the S2 domain or BAP and with streptavidin for the detection of biotinylation. The sizes and positions of marker proteins (in kilodalton) are indicated on the left.

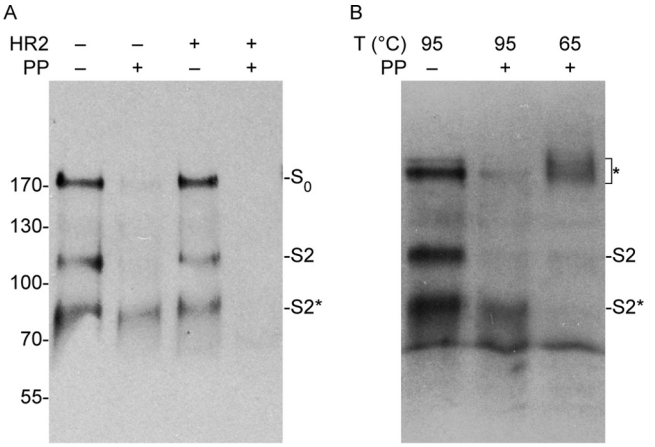

FIG 2 Detection of S protein after membrane fusion with target cells. (A) LR7-BirA cells were inoculated with MHV-BAP for 90 min in the absence or presence of peptidic fusion inhibitor (HR2) and lysed in the absence or presence of the BirA inhibitor PP. Immunoprecipitated S proteins were analyzed by Western blotting. Only biotinylated S protein was detected by streptavidin-HRP conjugate. Upon cell lysis in the absence of PP, all S protein was allowed to be biotinylated by BirA; thus, full-length S protein (S_0), S protein cleaved at the S1/S2 junction (S2), and a novel product of lower molecular mass designated S2* were detected. The presence of PP during lysis allowed the exclusive detection of S protein that was biotinylated during infection and mainly shows the S2* fragment. (B) IP samples were denatured at 95 or 65°C before Western blotting. In the presence of PP, the S2* fragment constitutes the majority of biotinylated S proteins migrating at ~80 kDa position. After heating IP samples at 65°C (instead of 95°C), a larger product was present around the ~200-kDa position (indicated by the asterisk).

synthetic peptide fusion inhibitor, which effectively blocks the membrane fusion activity of the S protein (11). Addition of the HR2 peptide efficiently abrogated biotinylation of the S protein in the presence of PP (Fig. 2A, lane 4). The experiment confirmed that biotinylation of S proteins only occurs after virus-cell fusion and further demonstrated that the proteolytic processing of S protein is not affected by the addition of the HR2 peptide (Fig. 2A, lane 3). We hypothesized that the S2* subunit represents the proteolytically primed subunit of MHV S protein.

The S2* subunit occurs in stable multimers. We examined the novel S2* subunit for characteristic features of the fusion machinery. To drive membrane fusion, the membrane-anchored domains of class I fusion proteins fold into a highly SDS-stable and temperature-resistant postfusion trimer, facilitated by the zipping up of the two HR domains into six-helix bundles (11, 34). To test whether S2* forms such stable trimers, we analyzed the SDS-PAGE migration of the biotinylated S protein variants after heat treatment of the samples at 65°C rather than at 95°C. The S2* subunit that was biotinylated upon infection of target cells migrated at ~80 kDa if denatured at 95°C. This species was, however, absent after denaturation at 65°C; instead, a larger band was observed at ~200 kDa, in line with the S2* subunit actually occurring as a stable, multimeric postfusion complex (Fig. 2B).

The kinetics of S2* appearance, virus cell fusion, and MHV infection coincide. If the novel S2* subunit represents the proteolytically primed form, the kinetics of S protein cleavage should be equal to or faster than productive MHV infection. We monitored the kinetics of S protein cleavage and fusion by performing a time course of infection with MHV-BAP on LR7-BirA cells. To synchronize infections, virus was allowed to bind to cells at 8°C for 1 h, followed by removal of the inoculum, after which infection was continued at 37°C. Omitting PP during the IP procedure revealed the overall biochemical fate of all (i.e., fused and nonfused) S proteins over a 90-min time period (Fig. 3A). Western blot anal-

Downloaded from http://jvi.asm.org/ on March 25, 2015 by Universiteitsbibliotheek Utrecht

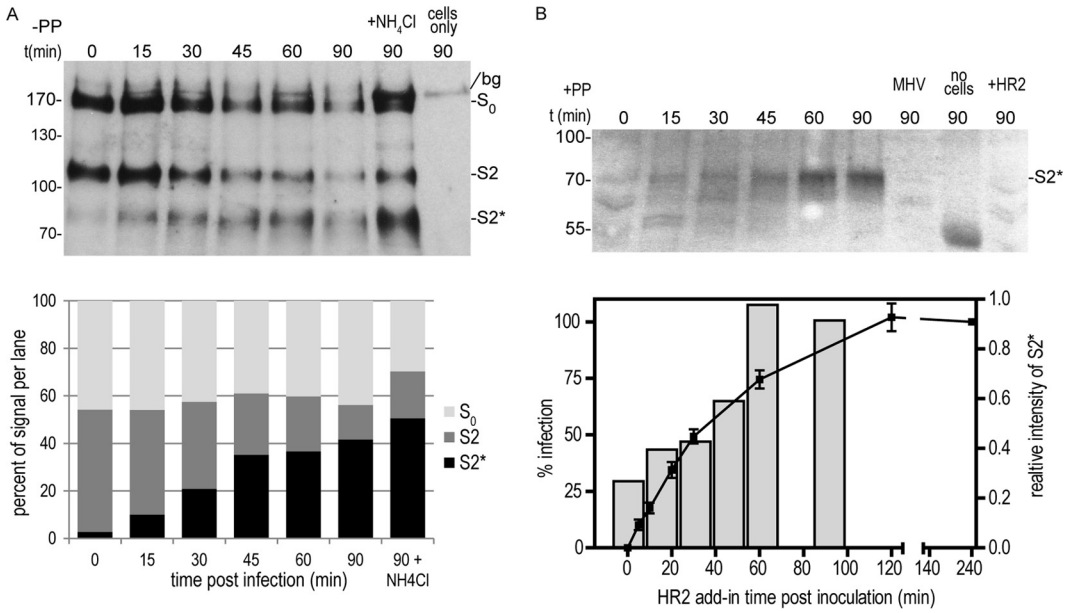

FIG 3 S2* fragment is generated during virus entry. (A) MHV-BAP was bound to LR7-BirA cells, and excess virus was removed to synchronize the infection. The infection was stopped at the indicated times postinfection by cell lysis in the absence of the BirA inhibitor PP. Immunoprecipitated S proteins were analyzed by Western blotting, and biotinylated protein was detected by using a streptavidin-HRP conjugate. To assess lysosomal degradation, ammonium chloride (NH_4Cl) was added during infection. A background band (bg) is indicated. The relative amounts of S_0, S2, and S2* protein per lane were quantified to illustrate the proteolytic processing over time (lower panel). (B) Same as panel A, except that by addition of PP during lysis, only S protein that has been biotinylated during infection was detected. As controls, MHV-BAP in the absence of cells, infection with wild-type MHV, and MHV-BAP infection performed in the presence of the HR2 fusion inhibitor were used. The intensity of the S2* fragment was quantified and is displayed as a bar diagram below. In addition, to determine the kinetics of virus entry independently, MHV infections were supplemented in time with the HR2 fusion inhibitor after a synchronized infection (line diagram). At 7 h p.i., infected cells were detected by immunostaining, and the relative amounts of infection were determined.

ysis of IP samples indicated that the relative amount of the S2* cleavage product increased over time, whereas the S_0 and S2 signal slowly vanished. To prevent the maturation of endosomes and the acidification of endolysosomal compartments, 25 mM NH_4Cl was added to the cells throughout infection (35). This treatment resulted in a net increase of S protein, suggesting that the time-dependent overall decrease in S protein in the absence of NH_4Cl was due to lysosomal degradation. In contrast, the proteolytic process leading to S2* formation was not blocked by NH_4Cl. Quantification of the density of the S protein bands over 90 min of infection showed that the fraction of the S2* subunit increased from 3 to 50% (Fig. 3A, bar chart). However, not all S proteins had undergone proteolytic processing after 90 min. By performing the analysis in the presence of PP during the sample preparation, only S protein from virus-cell fusion events was monitored (Fig. 3B). The appearance of the S2* subunit started early and continued increasingly for at least 90 min.

To confirm the kinetics of virus-cell fusion by an independent approach, we examined the inhibition of MHV infection by HR2 peptide fusion inhibitor. LR7 cells were pulse inoculated for 1.5 min with wild-type MHV to synchronize binding. Inocula were replaced by culture medium, after which HR2 peptide was added to individual samples at successive time points. The relative amount of infection was determined at 7 h p.i. by immune staining of the cells against MHV. The presence of HR2 peptide from the start completely abolished infection but showed no effect when added 120 min after inoculation (Fig. 3B, line chart). The MHV infection deduced from the HR2 peptide time-of-addition experiment showed similar kinetics to proteolysis of S protein yielding the S2* product but was slower. MHV infection coincided with the accumulation of the S2* subunit as monitored by intracellular biotinylation. In comparison, the intensities of the biotinylated S2* protein bands observed in the virus-cell fusion experiment were quantified and included in the same graph as a bar chart (Fig. 3B, bar chart).

Conserved arginine is not the cleavage site that yields the S2* subunit. The identification of the proteolytic cleavage site that yields the fusion active S2* subunit, could provide further information about the requirements for gaining fusion competence. Judged from the molecular weight of the S2* protein, the cleavage site is located within the N-terminal half of the S2 subunit. This region comprises a conserved arginine, previously described as a potential protease target site and termed S2′ in the S proteins of SARS-CoV and IBV (18, 36) (Fig. 4A). Cleavage at this arginine would truncate the S2 domain by ~15 kDa and remove two glycosylation sites, which is in agreement with the observed difference between the S2 and S2* band. We used a reverse-genetics approach to determine whether the MHV S2* subunit indeed results from proteolysis at the putative S2′ cleavage site. To that end, mutant MHV-BAP was generated containing two serine substitutions of arginines occurring at or close to the S2′ cleavage ($MHV^{S2'-}$BAP; Fig. 4A, table). Another MHV variant with a mutated furin cleavage site at the S1/S2 junction was generated by replacing the arginines by serines (MHV^{FCS-}BAP). Mutant viruses were viable and used to infect LR7-BirA cells for 90 min at an equal MOI, after which IP samples were prepared in the absence or presence of PP. Western blot analysis of IP samples showed that the knockout of the furin cleavage site at the S1/S2 junction in

Downloaded from http://jvi.asm.org/ on March 25, 2015 by Universiteitsbibliotheek Utrecht

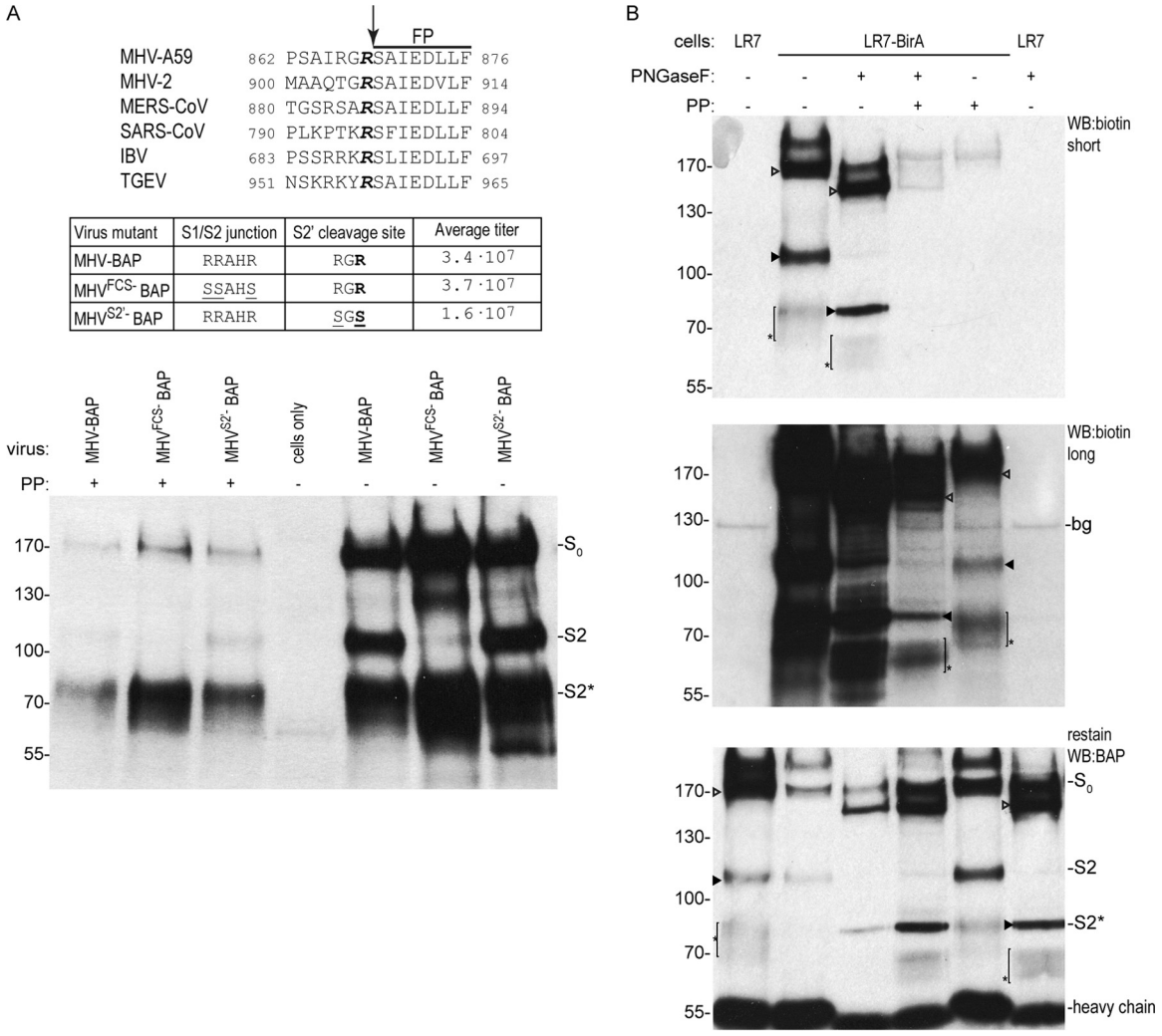

FIG 4 Characterization of the S2* fragment. (A) Sequence alignment of an S protein segment of representative CoVs containing the putative S2′ cleavage site (arrow) and part of the fusion peptide (FP). The conserved arginine residue adjacent to the putative fusion peptide (FP [37]) is indicated in boldface. The table shows the mutations of generated recombinant MHV viruses carrying serine substitutions of arginines (underlined) at the furin cleavage site at the S1/S2 junction (MHV^{FCS}-BAP) and the putative S2′ site (MHV$^{S2'}$-BAP). The average titer of three independent virus preparations was determined by endpoint dilution and is reported as the 50% tissue culture infective dose ($TCID_{50}$)/ml. BirA cells, infected with the recombinant viruses for 90 min, were lysed in the absence or presence of pyrophosphate (PP). Biotinylation of immunoprecipitated S proteins was detected by Western blotting, as described in the text. (B) Deglycosylation of biotinylated S proteins. The biotinylation assay was performed with MHV-BAP as described for panel A. Prior to Western blot analysis, all samples were denatured, and selected samples were subsequently deglycosylated using PNGase F. Biotinylated S protein was detected with streptavidin (two exposure times are shown), and the same blot was restained with anti-BAP antibody to detect (nonbiotinylated) S proteins (note that streptavidin binding to biotinylated BAP limits detection with the anti-BAP antibody). Full-length S protein is indicated by open triangles, S protein cleaved at the S1/S2 junction is indicated by solid triangles, and the S2* fragment is indicated by asterisks. All S proteins showed faster migration after deglycosylation; S_0 and S2 were reduced to a defined band upon deglycosylation, whereas the S2* fragment band remained diffuse. A cellular background band is indicated (bg).

MHV^{FCS}-BAP prevented the appearance of the S2 form (22) (Fig. 4A, lower panel). In contrast, serine substitution of the two arginines at the presumed S2′ cleavage site in MHV$^{S2'}$-BAP did not prevent the formation of the S2* subunit. When IP was performed in the presence of PP, only allowing the detection of the S proteins involved in fusion, the S2* subunit was clearly detected for all three viruses. The S2* product of the mutant viruses migrated with similar mobility and represented the major form of S protein that underwent fusion. Arginine substitutions at the S1/S2 or S2′ site had no detectable effect on virus titers, which remained comparable to MHV-BAP (Fig. 4A). As reported earlier, the deletion of the S1/S2 arginine motif resulted in reduced syncytium formation capacity of the virus (22).

Prediction of the S2′ cleavage site from the molecular weight of the S2* subunit after deglycosylation. Since we could not predict other protease cleavage sites from the S protein amino acid sequence, we tried to identify the S2′ cleavage site by alternative approaches. The biotinylation assay did not yield a sufficient amount and purity of the S2* subunit to allow N-terminal amino acid sequencing. Instead, we deglycosylated the S protein to more precisely determine the molecular weight of S2*, from which the approximate location of the cleavage site might then be deduced. To that end, LR7-BirA cells were inoculated with MHV-BAP for 90 min, and samples were prepared in the absence or presence of PP. After the IP, S protein bound to protein G-Sepharose beads was denatured, and samples were deglycosylated by PNGase F to

Downloaded from http://jvi.asm.org/ on March 25, 2015 by Universiteitsbibliotheek Utrecht

remove all N-linked glycans. Successful deglycosylation was revealed by the S proteins migrating with higher electrophoretic mobility (Fig. 4B, top and middle panel). Deglycosylation of all S proteins (−PP) and of S proteins from virions that had fused (+PP) showed a similar effect. The theoretical molecular masses were predicted to be 70 kDa for the S2 domain and 54 kDa for S2* if the cleavage occurs close to the putative FP. The deglycosylated S2 subunit shifted from the 105-kDa position to the 80-kDa position—slightly higher than predicted—and migrated as a well-defined band. In contrast, the S2* protein also shifted to a lower molecular mass, and yet it remained heterogeneous after deglycosylation, ranging in mass from 60 to 65 kDa. Similar to S2, the S2* subunit appears larger than its predicted molecular mass of 54 kDa; hence, cleavage may occur at the putative S2′ cleavage site or further upstream. The blot was restained with antiserum against the BAP in order to visualize the S proteins from infections of LR7 cell without BirA (Fig. 4B, lower panel) and independent of biotinylation. Of note, the prior streptavidin-biotin interaction reduces the anti-BAP antibody reactivity, particularly in fully biotinylated samples prepared in the absence of PP (Fig. 4B, lanes 2 and 3).

Inhibition of cellular proteases that generate the S2* subunit. To obtain information on the S protein cleavage site and the functional aspect of proteolysis during virus infection, we attempted to identify the responsible host cell proteases. SARS-CoV S protein can be cleaved by multiple proteases, and the availability of those proteases has been linked to the tissue tropism of the virus (7). However, expression of the MHV receptor can render cell lines of different species susceptible to MHV infection (31), and if the S2* subunit represents the fusion active form, the priming protease(s) should occur in various cell lines. To test this, we monitored S protein cleavage in nonmurine cell lines stably expressing the MHV receptor. Virus preparations containing prebiotinylated S protein were produced after a single passage on LR7-BirA (MHV-BAP*bio) and typically contained ca. 70% S_0, 30% S2, and a marginal fraction of S2* (Fig. 5A, lane 1). After 90 min of inoculation of two human and one simian cell line (i.e., HEK 293T, HeLa, and Vero cells, respectively), the patterns of S_0, S2, and S2* were similar compared to that in the murine LR7-BirA cell line (Fig. 5A). Broad-spectrum protease inhibitors can affect various classes of proteases. In order to characterize the proteases involved in S protein cleavage, a virus entry assay was performed in the presence of various protease inhibitors, suppressing the activity of the main classes of proteases. MHV-BAP infection was performed on LR7-BirA cells for 90 min in the presence of the cysteine protease inhibitor E64d, the metalloprotease inhibitor phosphoramidon, the aspartyl protease inhibitor pepstatin A, the serine and thiol protease inhibitor leupeptin, and the serine protease inhibitor AEBSF (Fig. 5B), as well as the serine protease inhibitor camostat or 1×-concentrated Roche mini-cocktail inhibitor (data not shown). In addition, the involvement of low-pH-dependent proteases was probed using the lysosomotropic agents NH_4Cl and bafilomycin A1 (Fig. 5C). None of the applied agents could prevent the S protein cleavage that results in the formation of the S2* subunit. The lysosomotropic agents NH_4Cl and bafilomycin A1 abolished fusion similar to the HR2 peptide fusion inhibitor, as indicated by the lack of biotinylated S when IP was performed in the presence of PP (Fig. 5C).

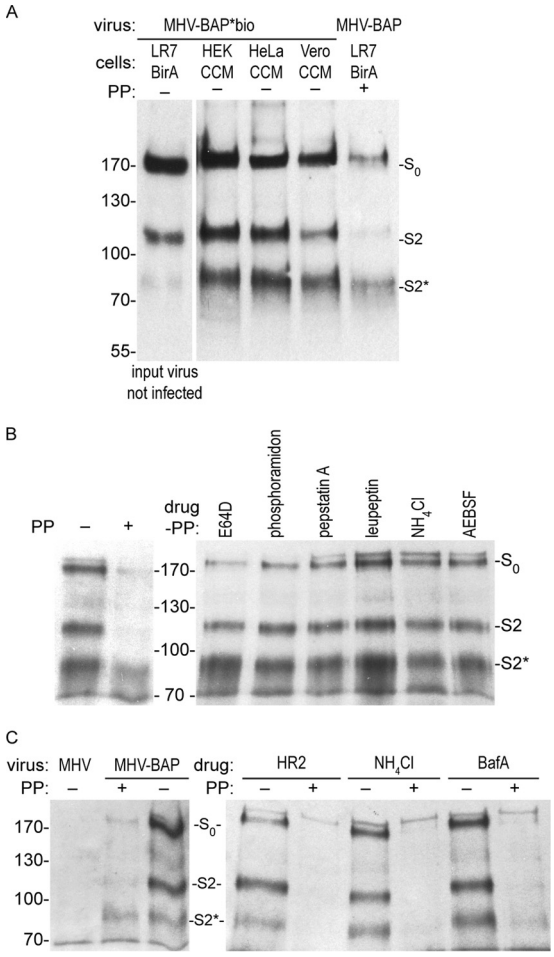

FIG 5 Protease inhibitors or lysosomotropic agents do not prevent S2* formation. (A) Biotinylated MHV-BAP (MHV-BAP*bio) progeny viruses were produced in LR7-BirA cells. Cells overexpressing the MHV receptor murine carcinoembryonic antigen-related cell adhesion molecule 1a (CCM) were infected with MHV-BAP*bio for 90 min. Immunoprecipitated S proteins were analyzed by Western blotting, and biotinylation was detected by using the streptavidin-HRP conjugate. The cleavage status of MHV-BAP*bio prior to infection was visualized by inoculating LR7-BirA with virus-containing cell culture supernatant for 2 h 15 min at 4°C and direct lysis without warming (first lane). (B) LR7-BirA target cells were pretreated with various broad-spectrum protease inhibitors for 30 min. Infection with MHV-BAP was allowed in the presence of protease inhibitors for 90 min, and sample preparation was subsequently performed in the absence of PP as described for panel A. (C) Same as panel B, except that infections were performed with MHV or MHV-BAP in the presence of HR2 fusion inhibitor, ammonium chloride (NH_4Cl), or bafilomycin A1 (BafA). Lysates were prepared in the absence or presence of PP.

DISCUSSION

We studied the cleavage of the MHV S glycoprotein during virus entry by an unbiased approach that allowed us to isolate fusion proteins of virions that accomplished virus-cell fusion, and we newly identified an S2* subunit. It displayed features of the fusion machinery, suggesting that the S2* subunit represents the fusion-active part of the S protein. In support of this, the majority of the postfusion S proteins were cleaved into the S2* protein and formed heat- and SDS-stable multimers that resemble the postfusion six-helix bundle. Furthermore, the kinetics of appearance of the biotinylated S2* protein coincided with the kinetics of virus

Downloaded from http://jvi.asm.org/ on March 25, 2015 by Universiteitsbibliotheek Utrecht

entry, as determined by monitoring the sensitivity of infection to the HR2 peptide fusion inhibitor. The size of the S2* protein indicates cleavage to occur in the S2′ region just upstream of the putative FP. We could not determine the exact cleavage site by reverse genetics, and the low mass amounts of the S2* protein did not allow its identification by mass spectrometry. Deglycosylation of the S2* protein resulted in a heterogeneous product, suggesting that cleavage can occur at alternative sites in proximity to the S2′ site. Protease inhibitors used to identify the protease responsible for S protein cleavage could not prevent the formation of the S2* subunit. Although the precise details of the cleavage process remain enigmatic, the appearance and characteristics of the S2* subunit support the idea that it represents the fusion-ready subunit.

Previous investigations of CoV fusion protein cleavage have monitored the infectivity of viruses or viruslike particles in the presence of protease inhibitors or after genetically modifying the fusion protein (14, 16, 21, 23, 36, 37). Many studies demonstrate cleavage of S proteins displayed on the cell surface by recombinant proteases, but only a few verify proteolysis in virus preparations upon exposure to recombinant proteases and soluble receptor (38, 39). These studies convincingly correlated cleavage of S protein with its membrane fusion capacity but failed to demonstrate cleavage during virus entry or identifying the fusion-competent subunit. In fact, the biochemical fate of viral glycoproteins on virions that are entering host cells at physiological MOIs is difficult to study. Given the limited amount of virus even at high MOIs, the significant fraction of noninfectious particles in each virus preparation, and the relatively low number of S proteins per virion, the specific detection of S proteins on successfully fusing virions is a great challenge. In the present study, we established a novel biochemical assay based on the conditional biotinylation of proteins to concentrate and purify MHV S proteins involved in functional virus-cell fusion events. This enables the identification and characterization of fused S proteins in combination with more classical experiments using site-directed mutagenesis and protease inhibitors. Our approach excludes contributions of nonfused virions and thus focuses on functional fusion events. Since the infecting virions take a physiological entry route, we do not rely on mimicking the fusion process by the addition of soluble receptor, exogenous protease treatment, or pH shock. The assay can be adapted to monitor the biochemical fate of structural virion components of any enveloped or nonenveloped virus upon entry.

The entry of various CoVs is supported by distinct proteases that can act at the plasma membrane of the target cell or in the endosomal compartments (10, 13). For MHV-A59, proteolytic processing at the S1/S2 junction enables efficient cell-cell fusion, resulting in syncytium formation (40), and mutagenesis of the cleavage site limits the syncytium size (23, 41). However, as we showed earlier (22) and confirmed here by substituting all arginines at the S1/S2 junction, the S1/S2 cleavage is dispensable for fusion activity and virus infectivity. This is supported by observations with a natural isolate, MHV-2 (42), or with a cell-passaged MHV/BHK isolate (43), which both lack a genuine furin cleavage site and hence carry uncleaved S proteins on their virions. In our study, only small amounts of the S2 subunit were present on virions that had fused, suggesting that S2 is not the fusion-active form. Nevertheless, cleavage of MHV S protein at the S1/S2 junction may provide additional structural flexibility to increase the accessibility of a cleavage site for priming, as suggested earlier for SARS-CoV (36). It is possible that S proteins are processed into S2*, perhaps via a short-lived intermediate S2 form that is not detected. With fewer priming proteases on the cell surface than in the endolysosomal compartments, this may explain the cell-cell fusion inability of the MHV spikes lacking a functional furin cleavage site.

We observed that S protein cleavage upon MHV infection occurred downstream of the S1/S2 junction and released an S2* fragment of ~80 kDa, which is ~25 kDa smaller than the S2 subunit. Assuming this membrane-bound subunit to carry the membrane fusion function, we probed the S2* subunit for criteria of the fusion machinery. First of all, the S2* subunit was the most abundant S protein species observed after virus-cell fusion and hence likely to be involved in membrane fusion. We assume that S_0 and S2 proteins decorate virions which failed to reach the cellular compartment where the appropriate stimuli and proteolytic activity occur for S protein activation. However, a limited number of virions reaches the fusion compartment, where a majority of S proteins are proteolytically processed and triggered for fusion. Second, S2* occurred in heat- and detergent-resistant multimers indicative of the characteristic class I postfusion six-helix bundle. Similarly, treatment of MHV-2 virions with soluble receptor, followed by protease treatment, revealed an equivalent pattern of S_0, S2, and S2* (38). Cathepsin L and trypsin cleaved the S protein, yielding a 71-kDa fragment that appeared as a stable, postfusion form, similar to S2* (38). Proteolytic priming of the MHV-2 S proteins upon virus entry was earlier implicated by studies with inhibitors of endolysosomal proteases and lysosomotropic agents and by trypsin bypass experiments, but the actual processing in cells was not confirmed (6). In our study, proteolytic processing of the S protein and virus-cell fusion, as measured by intracellular biotinylation of the S protein and by an independent virus infection assay, occurred with similar kinetics. The HR2 peptide fusion inhibitor prevents virus from fusion by inhibiting 6-helix bundle formation (11). Consistently, it also prevented S proteins of incoming virions from becoming biotinylated, allowing us to discriminate the sequential order of cleavage and fusion. If cleavage is a prerequisite for the S protein to mediate fusion, then HR2 must take effect after the proteolytic event, and HR2 peptide indeed did not affect the cleavage of S protein. We argue, based on these findings, that the S2* fragment fulfills the criteria of the functional fusion protein.

The difference in molecular weight between the S2 and S2* subunits predicts the suspected cleavage site to map ~230 amino acids downstream of the S1/S2 junction. Furthermore, priming of the class I fusion proteins often occurs directly N terminal of the FP, which has been described as a conserved sequence of apolar amino acids in the CoV S protein (16, 36, 37). Both predictions point toward two critical arginine residues in the MHV S2 domain and, intriguingly, cleavage at the same position (S2′) has been implicated to enable SARS-CoV S protein fusion (8, 10). By analogy, we suspected the S2′ cleavage site to be used in MHV-A59 S protein, but after mutagenesis of both arginines, the infectivity of MHV remained unaffected, and the S protein cleavage pattern upon fusion remained unaltered.

In an attempt to deduce the cleavage site from its molecular weight, we enzymatically removed the N-linked glycans of the S2* glycoprotein and analyzed its size. Although the deglycosylated S_0 and S2 proteins were reduced to sharply defined products, S2* remained ill defined, migrating as a heterogeneous band ranging from 60 to 65 kDa. Assuming that the S2 and S2* product under-

Downloaded from http://jvi.asm.org/ on March 25, 2015 by Universiteitsbibliotheek Utrecht

went similar posttranslational modifications, the variable size of the S2* fragment can be best explained by promiscuous proteolytic cleavages, whereas S2 is formed by cleavage precisely at the S1/S2 junction. Heterogeneity of cleavage products might result from a certain degree of plasticity of S2′ cleavage either by the existence of alternative cleavage sites or by involvement of multiple or alternative proteolytic enzymes, analogous to the fusion activation of the SARS-CoV S protein (13). The plasticity of the cleavage site also suggests that cleavage directly adjacent to the FP may not be an absolute requirement for fusion.

In our search for the cleavage site, we applied broad-spectrum protease inhibitors to identify corresponding (classes of) proteases. Testing protease inhibitors in SARS-CoV entry highlighted the involvement of cathepsin L and eventually led to the identification of the cathepsin L cleavage site in the S protein (15, 17). In contrast to SARS-CoV, the protease inhibitors leupeptin and E64d and specific cathepsin L/B inhibitors failed to block MHV-A59 infection (6, 14). We observed no effect on the proteolytic processing of MHV S proteins for broad-range protease inhibitors targeting cysteine, aspartyl, serine, thiol, and metallo proteases. We conclude that heterogeneity of the S2* subunit, our failure to knockout the S2′ cleavage site by mutation, and the insensitivity of MHV toward individual protease inhibitors are all consequences of redundant proteases and/or multiple cleavage sites that mediate MHV S protein priming. However, a given protease inhibitor may not block all individual proteases of a specific class, and our inhibitor panel was lacking threonine protease inhibitors and aminopeptidase inhibitors that potentially prime the S protein (44). Plasticity in cleavage is further supported by the similarity of S protein processing in various cell lines and may confer flexibility to the virus in infecting different tissues (45). Alternatively, heterogeneous S2* fragment could be explained in analogy to filovirus fusion protein processing, which requires gradual trimming by low-pH-activated endosomal proteases to reach fusion competence (46). However, we did not observe an enrichment of a particular S2* species over time, and lysosomotropic agents did not prevent cleavage. Nevertheless, MHV S protein priming is a distinct event that is timed after virus attachment and before lysosomal degradation. Binding to cells alone (Fig. 3A, time course) or incubation of virus preparations with cell lysates (data not shown) was not sufficient to trigger the cleavage event. On the other hand, the application of lysosomotropic agents, which can prevent endosome maturation at higher concentrations, prevented the S protein signal from declining over time. The quantification of the different S forms after 90 min of inoculation in the absence or presence of NH_4Cl indicated that this lysosomal degradation equally affects all forms of S but did not block cleavage into the S2* subunit. Hence, the S2* fragment is not the product of an unspecific lysosomal degradation processes but is cleaved by cellular proteases that are active prior to fusion and before degradation in the lysosomal system.

All class I viral fusion proteins have to minimally meet two requirements to accomplish fusion: proteolytic priming and triggering of membrane fusion. Priming by cleavage is a common maturation step to bring fusion proteins into the fusion-ready, metastable form (1, 2). Our data suggest that the S2* subunit represents primed MHV-A59 S protein and indicate, in combination with other observations, that many—if not all—CoV fusion proteins need cleavage to achieve the fusion-ready form (6, 8, 20, 39). In contrast to many typical class I fusion proteins, priming of S proteins does not occur in the producer cell; cleavage in the target cell provides an extra level of spatial and temporal control of virus fusion. Thus, MHV receptor-induced conformational changes are initiated at the target cell, exposing a proteolytic cleavage site (19, 38, 47). SARS CoV S proteins require a first cleavage to facilitate a consecutive cleavage that then renders the S protein fusion competent (36). Nevertheless, an additional trigger of unknown nature is probably necessary to initiate the membrane fusion, since we could block virus-cell fusion, using lysosomotropic agents, but not S protein cleavage. Low pH in the endolysosomal compartment may itself be a trigger but may as well be necessary for priming by low-pH-activated proteases (14, 48, 49). Triggers of an alternative nature seem, however, more likely because the infection of some CoVs can be bypassed using recombinant proteases without a pH decrease, whereas syncytium formation typically occurs at neutral pH (6, 20, 22, 39, 40). In summary, the priming of S proteins plays a pivotal role in the temporal and spatial regulation of CoV entry. With the conditional biotinylation assay described here, the priming events that occur after receptor binding and depend on cellular proteases can be characterized in detail.

ACKNOWLEDGMENTS

We acknowledge Zou Yong for kindly providing Vero CCL-81 cells.

This study was supported by EU Framework 7 program PITN-GA-2009-235649-Virus Entry.

REFERENCES

1. **Harrison SC.** 2008. Viral membrane fusion. Nat. Struct. Mol. Biol. **15:** 690–698. http://dx.doi.org/10.1038/nsmb.1456.
2. **White JM, Delos SE, Brecher M, Schornberg K.** 2008. Structures and mechanisms of viral membrane fusion proteins: multiple variations on a common theme. Crit. Rev. Biochem. Mol. Biol. **43:**189–219. http://dx.doi.org/10.1080/10409230802058320.
3. **Melikyan GB, Smith EC, Dutch RE.** 2012. Mechanisms of enveloped virus entry by membrane fusion, p 290–311. *In* Edward HE (ed), Comprehensive biophysics. Elsevier, Amsterdam, Netherlands.
4. **Epand RM.** 2003. Fusion peptides and the mechanism of viral fusion. Biochim. Biophys. Acta **1614:**116–121. http://dx.doi.org/10.1016/S0005-2736(03)00169-X.
5. **Chandran K, Sullivan NJ, Felbor U, Whelan SP, Cunningham JM.** 2005. Endosomal proteolysis of the Ebola virus glycoprotein is necessary for infection. Science **308:**1643–1645. http://dx.doi.org/10.1126/science.1110656.
6. **Qiu Z, Hingley ST, Simmons G, Yu C, Das Sarma J, Bates P, Weiss SR.** 2006. Endosomal proteolysis by cathepsins is necessary for murine coronavirus mouse hepatitis virus type 2 spike-mediated entry. J. Virol. **80:** 5768–5776. http://dx.doi.org/10.1128/JVI.00442-06.
7. **Bertram S, Heurich A, Lavender H, Gierer S, Danisch S, Perin P, Lucas JM, Nelson PS, Pohlmann S, Soilleux EJ.** 2012. Influenza and SARS-coronavirus activating proteases TMPRSS2 and HAT are expressed at multiple sites in human respiratory and gastrointestinal tracts. PLoS One **7:**e35876. http://dx.doi.org/10.1371/journal.pone.0035876.
8. **Kawase M, Shirato K, van der Hoek L, Taguchi F, Matsuyama S.** 2012. Simultaneous treatment of human bronchial epithelial cells with serine and cysteine protease inhibitors prevents severe acute respiratory syndrome coronavirus entry. J. Virol. **86:**6537–6545. http://dx.doi.org/10.1128/JVI.00094-12.
9. **Burri DJ, da Palma JR, Kunz S, Pasquato A.** 2012. Envelope glycoprotein of arenaviruses. Viruses **4:**2162–2181. http://dx.doi.org/10.3390/v4102162.
10. **Heald-Sargent T, Gallagher T.** 2012. Ready, set, fuse! The coronavirus spike protein and acquisition of fusion competence. Viruses **4:**557–580. http://dx.doi.org/10.3390/v4040557.
11. **Bosch BJ, van der Zee R, de Haan CA, Rottier PJ.** 2003. The coronavirus spike protein is a class I virus fusion protein: structural and functional characterization of the fusion core complex. J. Virol. **77:**8801–8811. http://dx.doi.org/10.1128/JVI.77.16.8801-8811.2003.
12. **de Haan CA, Haijema BJ, Schellen P, Wichgers Schreur P, te Lintelo E,**

Downloaded from http://jvi.asm.org/ on March 25, 2015 by Universiteitsbibliotheek Utrecht

Vennema H, Rottier PJ. 2008. Cleavage of group 1 coronavirus spike proteins: how furin cleavage is traded off against heparan sulfate binding upon cell culture adaptation. J. Virol. **82:**6078–6083. http://dx.doi.org/10.1128/JVI.00074-08.

13. **Belouzard S, Millet JK, Licitra BN, Whittaker GR.** 2012. Mechanisms of coronavirus cell entry mediated by the viral spike protein. Viruses **4:**1011–1033. http://dx.doi.org/10.3390/v4061011.
14. **Eifart P, Ludwig K, Bottcher C, de Haan CA, Rottier PJ, Korte T, Herrmann A.** 2007. Role of endocytosis and low pH in murine hepatitis virus strain A59 cell entry. J. Virol. **81:**10758–10768. http://dx.doi.org/10.1128/JVI.00725-07.
15. **Simmons G, Gosalia DN, Rennekamp AJ, Reeves JD, Diamond SL, Bates P.** 2005. Inhibitors of cathepsin L prevent severe acute respiratory syndrome coronavirus entry. Proc. Natl. Acad. Sci. U. S. A. **102:**11876–11881. http://dx.doi.org/10.1073/pnas.0505577102.
16. **Watanabe R, Matsuyama S, Shirato K, Maejima M, Fukushi S, Morikawa S, Taguchi F.** 2008. Entry from the cell surface of severe acute respiratory syndrome coronavirus with cleaved S protein as revealed by pseudotype virus bearing cleaved S protein. J. Virol. **82:**11985–11991. http://dx.doi.org/10.1128/JVI.01412-08.
17. **Bosch BJ, Bartelink W, Rottier PJ.** 2008. Cathepsin L functionally cleaves the severe acute respiratory syndrome coronavirus class I fusion protein upstream of rather than adjacent to the fusion peptide. J. Virol. **82:**8887–8890. http://dx.doi.org/10.1128/JVI.00415-08.
18. **Yamada Y, Liu DX.** 2009. Proteolytic activation of the spike protein at a novel RRRR/S motif is implicated in furin-dependent entry, syncytium formation, and infectivity of coronavirus infectious bronchitis virus in cultured cells. J. Virol. **83:**8744–8758. http://dx.doi.org/10.1128/JVI.00613-09.
19. **Matsuyama S, Taguchi F.** 2002. Receptor-induced conformational changes of murine coronavirus spike protein. J. Virol. **76:**11819–11826. http://dx.doi.org/10.1128/JVI.76.23.11819-11826.2002.
20. **Sturman LS, Ricard CS, Holmes KV.** 1985. Proteolytic cleavage of the E2 glycoprotein of murine coronavirus: activation of cell-fusing activity of virions by trypsin and separation of two different 90K cleavage fragments. J. Virol. **56:**904–911.
21. **Bos EC, Luytjes W, Spaan WJ.** 1997. The function of the spike protein of mouse hepatitis virus strain A59 can be studied on virus-like particles: cleavage is not required for infectivity. J. Virol. **71:**9427–9433.
22. **de Haan CA, Stadler K, Godeke GJ, Bosch BJ, Rottier PJ.** 2004. Cleavage inhibition of the murine coronavirus spike protein by a furin-like enzyme affects cell-cell but not virus-cell fusion. J. Virol. **78:**6048–6054. http://dx.doi.org/10.1128/JVI.78.11.6048-6054.2004.
23. **Gombold JL, Hingley ST, Weiss SR.** 1993. Fusion-defective mutants of mouse hepatitis virus A59 contain a mutation in the spike protein cleavage signal. J. Virol. **67:**4504–4512.
24. **Kuo L, Godeke GJ, Raamsman MJ, Masters PS, Rottier PJ.** 2000. Retargeting of coronavirus by substitution of the spike glycoprotein ectodomain: crossing the host cell species barrier. J. Virol. **74:**1393–1406. http://dx.doi.org/10.1128/JVI.74.3.1393-1406.2000.
25. **Janes PW, Griesshaber B, Atapattu L, Nievergall E, Hii LL, Mensinga A, Chheang C, Day BW, Boyd AW, Bastiaens PI, Jorgensen C, Pawson T, Lackmann M.** 2011. Eph receptor function is modulated by heterooligomerization of A and B type Eph receptors. J. Cell Biol. **195:**1033–1045. http://dx.doi.org/10.1083/jcb.201104037.
26. **Taguchi F, Shimazaki YK.** 2000. Functional analysis of an epitope in the S2 subunit of the murine coronavirus spike protein: involvement in fusion activity. J. Gen. Virol. **81:**2867–2871.
27. **de Haan CA, Haijema BJ, Masters PS, Rottier PJ.** 2008. Manipulation of the coronavirus genome using targeted RNA recombination with interspecies chimeric coronaviruses. Methods Mol. Biol. **454:**229–236. http://dx.doi.org/10.1007/978-1-59745-181-9_17.
28. **Beckett D, Kovaleva E, Schatz PJ.** 1999. A minimal peptide substrate in biotin holoenzyme synthetase-catalyzed biotinylation. Protein Sci. **8:**921–929.
29. **Rossen JW, Bekker CP, Strous GJ, Horzinek MC, Dveksler GS, Holmes KV, Rottier PJ.** 1996. A murine and a porcine coronavirus are released from opposite surfaces of the same epithelial cells. Virology **224:**345–351. http://dx.doi.org/10.1006/viro.1996.0540.
30. **Mechold U, Gilbert C, Ogryzko V.** 2005. Codon optimization of the BirA enzyme gene leads to higher expression and an improved efficiency of biotinylation of target proteins in mammalian cells. J. Biotechnol. **116:**245–249. http://dx.doi.org/10.1016/j.jbiotec.2004.12.003.
31. **Dveksler GS, Pensiero MN, Cardellichio CB, Williams RK, Jiang GS, Holmes KV, Dieffenbach CW.** 1991. Cloning of the mouse hepatitis virus (MHV) receptor: expression in human and hamster cell lines confers susceptibility to MHV. J. Virol. **65:**6881–6891.
32. **Ng B, Polyak SW, Bird D, Bailey L, Wallace JC, Booker GW.** 2008. *Escherichia coli* biotin protein ligase: characterization and development of a high-throughput assay. Anal. Biochem. **376:**131–136. http://dx.doi.org/10.1016/j.ab.2008.01.026.
33. **Laemmli UK.** 1970. Cleavage of structural proteins during the assembly of the head of bacteriophage T4. Nature **227:**680–685. http://dx.doi.org/10.1038/227680a0.
34. **Miura HS, Nakagaki K, Taguchi F.** 2004. N-terminal domain of the murine coronavirus receptor CEACAM1 is responsible for fusogenic activation and conformational changes of the spike protein. J. Virol. **78:**216–223. http://dx.doi.org/10.1128/JVI.78.1.216-223.2004.
35. **Ohkuma S, Chudzik J, Poole B.** 1986. The effects of basic substances and acidic ionophores on the digestion of exogenous and endogenous proteins in mouse peritoneal macrophages. J. Cell Biol. **102:**959–966. http://dx.doi.org/10.1083/jcb.102.3.959.
36. **Belouzard S, Chu VC, Whittaker GR.** 2009. Activation of the SARS coronavirus spike protein via sequential proteolytic cleavage at two distinct sites. Proc. Natl. Acad. Sci. U. S. A. **106:**5871–5876. http://dx.doi.org/10.1073/pnas.0809524106.
37. **Madu IG, Roth SL, Belouzard S, Whittaker GR.** 2009. Characterization of a highly conserved domain within the severe acute respiratory syndrome coronavirus spike protein S2 domain with characteristics of a viral fusion peptide. J. Virol. **83:**7411–7421. http://dx.doi.org/10.1128/JVI.00079-09.
38. **Matsuyama S, Taguchi F.** 2009. Two-step conformational changes in a coronavirus envelope glycoprotein mediated by receptor binding and proteolysis. J. Virol. **83:**11133–11141. http://dx.doi.org/10.1128/JVI.00959-09.
39. **Matsuyama S, Ujike M, Morikawa S, Tashiro M, Taguchi F.** 2005. Protease-mediated enhancement of severe acute respiratory syndrome coronavirus infection. Proc. Natl. Acad. Sci. U. S. A. **102:**12543–12547. http://dx.doi.org/10.1073/pnas.0503203102.
40. **Frana MF, Behnke JN, Sturman LS, Holmes KV.** 1985. Proteolytic cleavage of the E2 glycoprotein of murine coronavirus: host-dependent differences in proteolytic cleavage and cell fusion. J. Virol. **56:**912–920.
41. **Bos EC, Heijnen L, Luytjes W, Spaan WJ.** 1995. Mutational analysis of the murine coronavirus spike protein: effect on cell-to-cell fusion. Virology **214:**453–463. http://dx.doi.org/10.1006/viro.1995.0056.
42. **Yamada YK, Takimoto K, Yabe M, Taguchi F.** 1997. Acquired fusion activity of a murine coronavirus MHV-2 variant with mutations in the proteolytic cleavage site and the signal sequence of the S protein. Virology **227:**215–219. http://dx.doi.org/10.1006/viro.1996.8313.
43. **de Haan CA, Li Z, te Lintelo E, Bosch BJ, Haijema BJ, Rottier PJ.** 2005. Murine coronavirus with an extended host range uses heparan sulfate as an entry receptor. J. Virol. **79:**14451–14456. http://dx.doi.org/10.1128/JVI.79.22.14451-14456.2005.
44. **Lopez-Otin C, Bond JS.** 2008. Proteases: multifunctional enzymes in life and disease. J. Biol. Chem. **283:**30433–30437. http://dx.doi.org/10.1074/jbc.R800035200.
45. **Slobodskaya O, Snijder EJ, Spaan WJ.** 2012. Organ tropism of murine coronavirus does not correlate with the expression levels of the membrane-anchored or secreted isoforms of the carcinoembryonic antigen-related cell adhesion molecule 1 receptor. J. Gen. Virol. **93:**1918–1923. http://dx.doi.org/10.1099/vir.0.043190-0.
46. **Hunt CL, Lennemann NJ, Maury W.** 2012. Filovirus entry: a novelty in the viral fusion world. Viruses **4:**258–275. http://dx.doi.org/10.3390/v4020258.
47. **Holmes KV, Zelus BD, Schickli JH, Weiss SR.** 2001. Receptor specificity and receptor-induced conformational changes in mouse hepatitis virus spike glycoprotein. Adv. Exp. Med. Biol. **494:**173–181. http://dx.doi.org/10.1007/978-1-4615-1325-4_29.
48. **Sturman LS, Ricard CS, Holmes KV.** 1990. Conformational change of the coronavirus peplomer glycoprotein at pH 8.0 and 37°C correlates with virus aggregation and virus-induced cell fusion. J. Virol. **64:**3042–3050.
49. **Zelus BD, Schickli JH, Blau DM, Weiss SR, Holmes KV.** 2003. Conformational changes in the spike glycoprotein of murine coronavirus are induced at 37°C either by soluble murine CEACAM1 receptors or by pH 8. J. Virol. **77:**830–840. http://dx.doi.org/10.1128/JVI.77.2.830-840.2003.

Downloaded from http://jvi.asm.org/ on March 25, 2015 by Universiteitsbibliotheek Utrecht